Available online at www.sciencedirect.com
ScienceDirect
Ceramics International 36 (2010) 1075–1082
CERAMICS INTERNATIONAL
www.elsevier.com/locate/ceramint

Microstructure evaluation of sintered combustion-derived fine powder NiO–YSZ

Marjan Marinšek, Klementina Zupan *

Faculty of Chemistry and Chemical Technology, University of Ljubljana, Aškerčeva 5, 1000 Ljubljana, Slovenia

Received 9 September 2009; received in revised form 26 October 2009; accepted 22 November 2009
Available online 4 January 2010

Abstract

Citrate–nitrate combustion synthesis was used for the preparation of NiO–YSZ. The main advantage of the preparation method used was reflected in the fact that after the synthesis both phases NiO and YSZ were randomly distributed on a nanometre level. The prepared NiO–YSZ powder composites were shaped, sintered and reduced to Ni–YSZ and subsequently submitted to microstructure investigations. Relative sintered densities higher than 90% were obtained at sintering temperatures as low as 1200 °C. A sintering temperature 1200 °C was also recognized as the preparation temperature that provided the smallest Ni grains in the final Ni–YSZ cermet with an average Ni-particle diameter as low as 0.27 μm.

Keywords: A. Powders-chemical preparation; B. Nanocomposites; B. Microstructure; E. Fuel cells; Ni–YSZ

1. Introduction

Due to their high efficiency and environmental friendly nature, solid oxide fuel cells (SOFCs) are considered to be one of the most promising energy converters for the future [1,2]. The requirements of any potential electrode material in a SOFC are high electronic and ionic conductivity, stability under operating conditions, chemical and thermal expansion compatibility with other cell components, electrochemical activity and appropriate microstructure [3–5]. Nickel–yttria-stabilized zirconia cermets (Ni–YSZ) are, despite some drawbacks related with long term stability, the most widely adopted materials for SOFC anodes, mainly due to their good electrocatalytic properties against low price [6,7].

In general, at the anode site, fuel gas is electrochemically oxidized at the Ni–YSZ–fuel interface, called the triple phase boundary (TPB) region. It is well known that the higher the TPB length, the better electrochemical activity of the anode [8,9]. Therefore, both the activity of Ni–YSZ and their stability are strongly influenced by the cermets' morphology and microstructures such as grain connectivity, grain size, pore size and pore size distribution [10,11]. Many papers have been published describing different approaches to the microstructure optimization of Ni–YSZ cermets [12–14] and they seem to have one common aim: the need for nano-sized cermet composition. Specifically, according to the percolation theory, the electrical conductivity of two-phase composites is determined by the size and shape of particles as well as their volumetric fraction [15]. Finer conductive particles tend to be percolated through the composite material at lower concentrations and lower sintering temperatures, thus resulting in higher freedom in tailoring the Ni–YSZ composition. It was also reported that very homogeneous and ultrafine-Ni–YSZ mixtures enable both improved current–potential characteristics and enhanced initial stability of the electrochemical performance [16,17]. The increased electrochemical activity of very fine Ni–YSZ mixtures is understood in terms of increased TPB length [18,19]. The porosity of the anode cermet, often regarded as a third insulating phase, is another very important microstructure characteristic. Since porosity in Ni–YSZ cermet is mainly formed during the final stages of the cermet preparation (reduction of NiO to metallic Ni), it is reasonable to predict that uniform porosity with controlled pore size distribution can be achieved from NiO–YSZ mixtures initially formed of nano-sized particles.

In order to prepare Ni–YSZ cermets composed of ultrafine particles, conventional methods, such as mechanical mixing and ball milling, are no longer appropriate. Therefore, the development of a process, as cheap and as simple as possible,

* Corresponding author. Tel.: +386 1 2419 208; fax: +386 1 2419 220.
E-mail address: klementina.zupan@fkkt.uni-lj.si (K. Zupan).

0272-8842/$36.00
doi:10.1016/j.ceramint.2009.12.014

leading to produce porous anode layers containing nano-sized mixed particles is an intensively investigated objective. Several routes, such as coprecipitation [20,21], spray pyrolysis [22] and aerosol flame deposition [23] have been used to prepare small particle-sized powders but the preparation of complex metal oxides by combustion synthesis has recently become an important area of research due the promising results of this technique compared to the conventional method [24,25]. The main advantage of combustion synthesis is the ability to produce complex oxide powders directly from the precursor solution. Therefore, the combustion synthesis could be, in principle, a good method for preparing the composite powder of Ni–YSZ with uniform distribution of fine Ni particles within the YSZ framework. In this respect, combustion synthesis for Ni–YSZ cermet preparation has already been successfully applied by some authors. Ringuede et al. [26] established the reaction system employing nitrate as oxidizing reagent and urea as the fuel component. Aruna et al. [27] prepared Ni–YSZ cermet powder using carbohydrazide as the fuel component, while Kim et al. [28] based the combustion system on the nitrate–glycine reaction.

The aim of this work is to demonstrate that nano-scaled highly sinterable NiO–YSZ dispersions can be prepared using combustion synthesis technique. High sinterability of the prepared powders is of prime importance for the preparation of dense bodies at relatively low temperatures (below 1200 °C). With a detailed examination of the densification process of such ceramic powders and compact characteristics, we also demonstrated microstructure evolution from synthesized NiO–YSZ nano-powder to Ni–YSZ anode cermet.

2. Experimental procedure

NiO–YSZ composite powders were prepared with a modified combustion synthesis. The combustion system was based on the citrate–nitrate redox reaction. In this combustion method, the starting materials were $ZrO(NO_3)_2{\cdot}6H_2O$, $Ni(NO_3)_2{\cdot}6H_2O$, $Y(NO_3)_3{\cdot}6H_2O$, nitric acid (65%), and citric acid (analytical reagent grade). All solid compounds were dissolved with minimum additions of water in the amounts that assure the desired Ni content in final cermet (50 vol.% Ni). $ZrO(NO_3)_2{\cdot}6H_2O$ and $Y(NO_3)_3{\cdot}6H_2O$ additions were calculated to assure final YSZ composition to be $Zr_{0.85}Y_{0.15}O_{1.93}$. The five-reactant solutions were mixed together to prepare the reaction mixture and then treated under vacuum (20 mmHg) at 60 °C until the solution transformed into a bright green gel. Typical amounts of precursors used in one batch were 4.764 g $ZrO(NO_3)_2{\cdot}6H_2O$, 14.989 g $Ni(NO_3)_2{\cdot}6H_2O$, 0.936 g $Y(NO_3)_3{\cdot}6H_2O$, 7.369 g $C_6H_8O_7{\cdot}H_2O$, and 4 mL HNO_3. The gel was then gently milled in an agate mortar and uniaxially pressed (17 MPa) into pellets (ϕ = 12 mm, height ~30 mm). Such samples were placed on a corundum plate and ignited at the top of the pellet (Fig. 1). A rapid increase in temperature inside the reaction zone was visually observed, and also measured as temperature profile using an optical pyrometer (Ircon, IPE 140, based on sample brightness). The measuring range of this pyrometer is from 50 to 1200 °C and it has a very quick response time (1.5 ms). The accuracy of optically measured temperature was ±2.5 °C below 400 °C and ±0.4% of a measured value (in °C) above 400 °C. High temperatures were reached in a short reaction time by the self-generated heat of the reaction, yielding nano-powders or loose agglomerates of nano-crystallites. The peak temperature reached during the synthesis was measured as 1153 °C and the wave velocity 0.5 mm s^{-1}. The samples cooled down from their peak temperature to 50 °C in approximately 80 s. The grain size of both phases in the synthesized composite material (prior to attritor milling) was investigated by TEM (JEM-2010F TEM/STEM, operated at 200 keV, equipped with an URP pole-piece (C_S = 0.48 mm), EDS and PEELS). The powders for TEM microscopy were gently crushed in an agate mortar. A dilute suspension was prepared in absolute alcohol. A drop of the suspension was deposited on a holey carbon-coated copper grid, which was subsequently dried. In the TEM mode, both bright-field (BF) and dark-field (DF) images were recorded with the corresponding electron diffraction patterns (SAED).

After the synthesis, the powders were milled in attritor mill (4 h). The samples were then used for green body preparation and microstructure development tests during sintering. Particle size distribution of both attritor-milled and unmilled samples

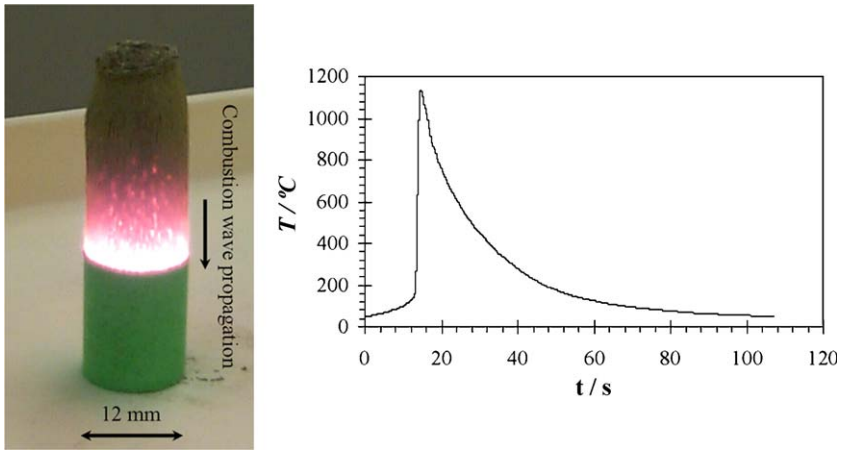

Fig. 1. Photograph of a typical citrate–nitrate gel combustion process for NiO–YSZ preparation together with typical temperature profile measured in a single spot.

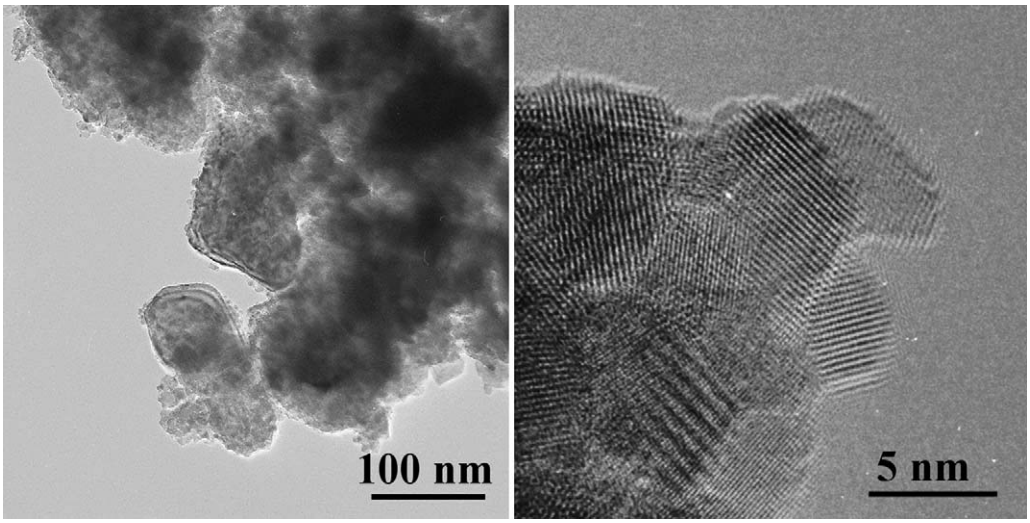

Fig. 2. Bright-field (BF) low magnification TEM image of the as reacted sample (left picture) and HRTEM image of the as reacted sample (right picture).

were measured using a MICROTRAC S 3500 particle sizer. For sinterability tests, milled samples were uniaxially pressed into pellets (100 MPa) and sintered at different temperatures (1150 °C, 1200 °C, 1250 °C, 1300 °C, 1350 °C, 1400 °C). Material shrinkage during sintering was measured separately using a LEITZ WETZLAR heating microscope. For microstructure determination, sintered tablets were polished (diamond paste 3 and 0.25 μm), thermally etched, reduced at 900 °C (2 h) in H_2/Ar atmosphere and subsequently analyzed with a SEM (Zeiss FE SUPRA 35 VP). Phase compositions of the samples were analyzed by EDS, supported by INCA software (Oxford Instruments). The quantitative analysis of the microstructures was performed on digital images (images were digitized into pixels with 255 different gray values using Zeiss KS300 3.0 image-analysis software).

3. Results and discussion

One of the main advantages of the combustion synthesis is its self-sustaining heat generation, which enables rapid heating of a reaction system. That means combustion synthesis takes just a few seconds to turn a mixture of reactants into a new solid, as opposed to the much longer time required for the same process to be conducted in an oven as solid state reaction. In the case of the NiO–YSZ citrate–nitrate combustion synthesis, the maximum temperature gradient inside the reaction zone (calculated on a basis of the temperature profile measurements) was 1164 K s^{-1}. Such a high temperature gradient and short reaction times resulted in a unique powder mixture composed of nano-sized partially agglomerated particles (Fig. 2). According to TEM investigations, these nano-particles are a random mixture of NiO and YSZ. The average measured crystallite size estimated from the HRTEM image for the two phases was 6.5 ± 2 nm. Such an oxide mixture was the starting material for the final Ni–YSZ cermet preparation.

The ideal microstructure of the final Ni–YSZ cermet is composed of very small grains of both phases (preferably submicrometer or nano-sized) in order to increase the TPB length. In contrast, Ni–YSZ also has to exhibit continuity of both phases throughout the cermet, since it must serve both as an electronically and ionically conductive material. High conductivity, in principle, is achieved when good contact between particles is ensured; this is normally accomplished through sintering. However, sintering also means grain growth, which is in contradiction to the desire to preserve NiO–YSZ nanodistribution. However, if the sintering temperatures required for NiO–YSZ densification can be lowered, then fine oxide mixtures can also be preserved in the sintered structures.

The sintering temperature of the prepared NiO–YSZ mixture was influenced by milling it in the attritor. Since a relatively large amount of volatile products are released during the citrate–nitrate combustion [29,30], NiO–YSZ after the synthesis is composed of soft agglomerates, which can be easily reduced in size. The main agglomerate size before and after attritor milling was 25.72 μm and 0.28 μm, respectively; expressed with specific surface area, it increased from 4.7 m^2/g in the unmilled sample to 22.0 m^2/g in attritor-milled sample.

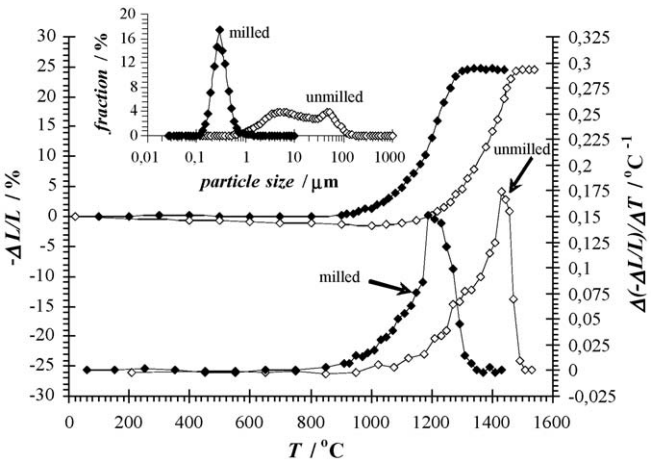

Fig. 3. Relative linear shrinkage and shrinkage rate versus temperature of unmilled and milled samples, respectively, together with particle size distribution in unmilled and milled samples.

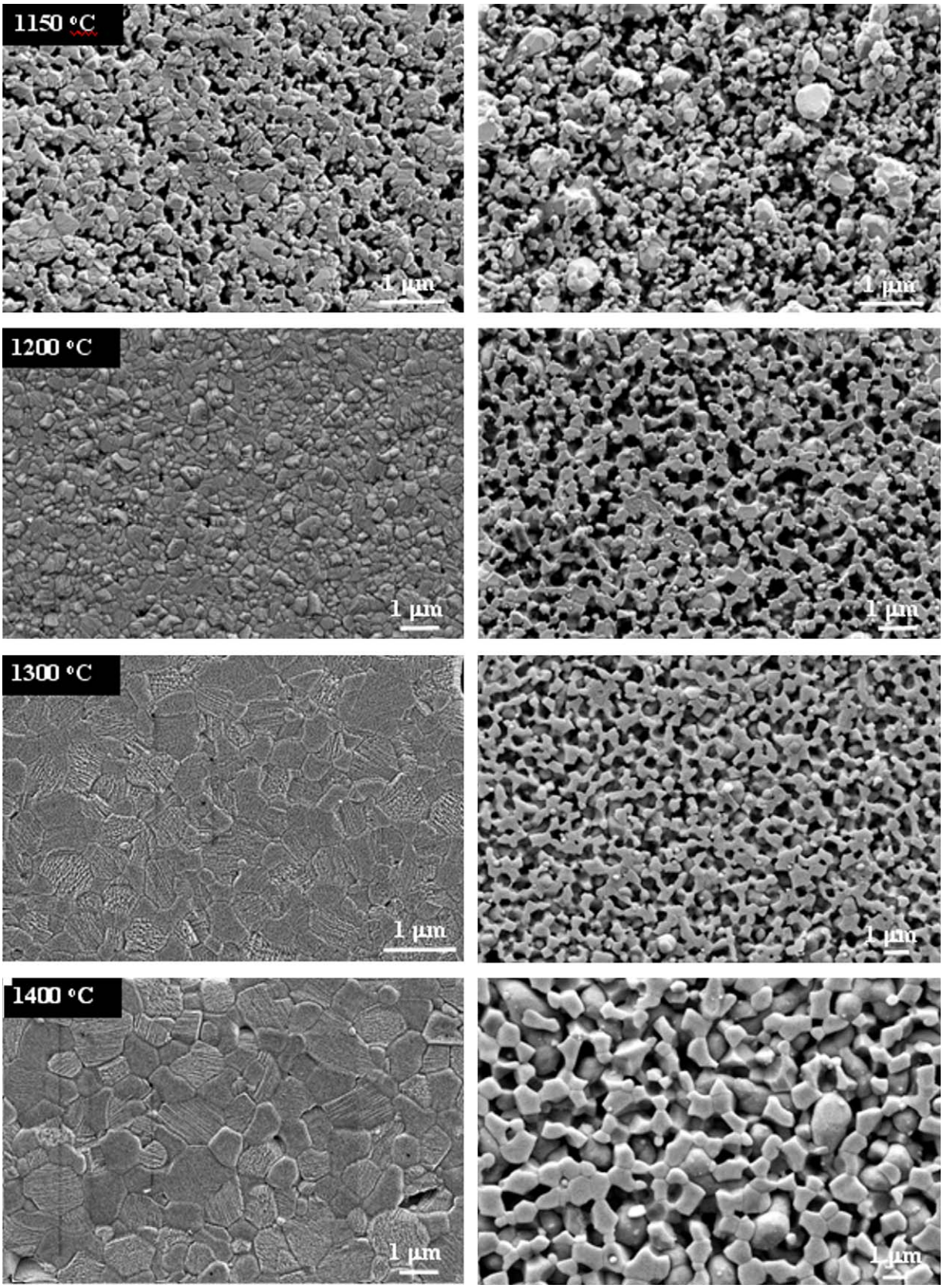

Fig. 4. SEM micrographs of samples obtained after sintering and subsequent reduction of NiO–YSZ green bodies (mind that magnification bars are not identical).

An effect of agglomerate size reduction on sintering temperature is presented in Fig. 3. Besides essentially lower sintering temperature (determined as 1200 °C for attritor-milled sample and 1420 °C for unmilled sample), shrinkage in the attritor-milled sample can be described with only one densification process as illustrated with the shrinkage rate curve. Contrarily, unmilled sample sinters through several stages with different shrinkage rates as a result of inter- and/or intra-agglomerate sintering.

The relatively low sintering temperature determined for attritor-milled sample may be very important from the applicability point of view. Specifically, due to the fact that lanthanum–strontium–manganite (LSM) cathode material may react with YSZ electrolyte at temperatures above 1200 °C forming a poorly conductive $La_2Zr_2O_7$ phase [31], a single cell is normally prepared through several sintering processes. First, the anode and electrolyte layers are co-sintered at higher temperatures (up to 1400 °C) and then the cathode layer is applied and co-sintered at temperatures up to 1200 °C. Successful sintering of NiO–YSZ anode material at temperatures below 1200 °C may result in a diverse SOFC preparation procedure, in which all layers are co-sintered in a single step.

In order to obtain more detailed information about the microstructure development, NiO–YSZ green bodies prepared from the attritor-milled powder were sintered under various sintering conditions. Sintering temperatures were defined according to the obtained shrinkage curve. The presented microstructures (Fig. 4) revealed that the nano-sized oxide mixture was no longer present in the sintered cermets. Instead, the one-phase dominance grew but remained well within the sub-micrometer range if the cermets had been sintered at relatively low temperatures. Additionally, it is evident that a relatively dense structure can be prepared using sintering temperatures no higher than 1200 °C. This is important because dense structures after sintering also ensure good contact between particles and continuity of both phases. Continuity of phases is essential not only with regard to conductivity, but also for microstructure stability. One good example of the insufficiently stable NiO–YSZ microstructure is shown in the case of sample A (sintered at 1150 °C). Although in this case grains of both phases were the smallest after sintering, compared to other investigated samples, the situation changed when the sintered sample was reduced. During the reduction, newly formed metallic Ni particles showed excessive grain growth. This phenomenon is a consequence of the fairly different surface energy of Ni and YSZ, which causes the hetero-grains at the interface to lose chemical affinity. Consequently, coarsening of the Ni phase proceeds appreciably due to poor adhesion of the metal to the ceramic material at elevated temperatures. From a practical point of view, excessive growth of the Ni grains results in the TPB length reduction. It is also realistic to expect that cermets whose morphology changes so much during the NiO reduction will undergo major microstructure modifications also in any potential long term use in SOFC. In all other samples (B to F), the grain growth of both phases (also in the reduced state) was controlled predominantly with the sintering temperature and no excessive enlargement of Ni grains after the reduction was noticed. Some microstructure parameters related to the sintering and reduction processes are summarized in Table 1.

Since all microstructure parameters important for exact cermet analysis are sometimes difficult to deduce simply from SEM micrographs, a detailed quantitative microstructure analysis on sintered and reduced samples was performed. For statistically reliable data in each case, 5–10 different regions were analyzed. The results of the quantitative

Table 1
Sintering parameters of various NiO–YSZ tablets.

Sample	T_{sintr} (°C)	$\Delta L/L$ (%)			ρ_{rel} (%)	
		Diameter	Height	Density	Sintered state	Reduced state
A	1150	15.2	15.3	15.2	72.6	55.3
B	1200	21.7	20.6	21.2	91.4	70.9
C	1250	23.2	22.5	22.4	96.4	73.4
D	1300	23.2	22.8	22.7	97.7	74.3
E	1350	23.3	22.3	22.7	95.8	73.5
F	1400	22.9	22.2	22.4	95.2	73.8

Table 2
Quantitative microstructure analysis of the sintered samples.

Sample	Porosity, ε (%)		$\bar{d}$ (μm)			Shape factor, ψ			d_x (μm)			d_y (μm)		
	Geometrical	Microstructural	NiO	YSZ	Pores	NiO	YSZ	Pores	NiO	YSZ	Pores	NiO	YSZ	pores
A	27.4	27.3	0.10	0.10	0.16	0.79	0.78	0.49	0.11	0.11	0.21	0.11	0.10	0.23
B	9.6	8.6	0.23	0.17	0.24	0.80	0.80	0.55	0.26	0.18	0.28	0.27	0.20	0.30
C	3.6	3.2	0.37	0.31	0.39	0.83	0.81	0.59	0.40	0.32	0.40	0.40	0.34	0.39
D	2.3	2.5	0.42	0.43	0.56	0.83	0.81	0.53	0.48	0.42	0.49	0.47	0.43	0.47
E	2.2	1.7	0.54	0.53	0.68	0.86	0.82	0.58	0.59	0.55	0.54	0.58	0.49	0.53
F	2.8	1.7	0.76	0.69	0.68	0.78	0.75	0.56	0.86	0.69	0.79	0.87	0.71	0.73

Table 3
Quantitative microstructure analysis of the reduced samples.

Sample	Porosity, ε (%)		$\bar{d}$ (μm)			Shape factor, ψ			d_x (μm)			d_y (μm)		
	Geometrical	Microstructural	Ni	YSZ	Pores	Ni	YSZ	Pores	Ni	YSZ	Pores	Ni	YSZ	Pores
A	44.7	41.2	0.44	0.10	0.16	0.78	0.80	0.54	0.46	0.12	0.19	0.49	0.12	0.24
B	30.1	29.9	0.27	0.17	0.19	0.83	0.80	0.53	0.29	0.20	0.30	0.28	0.18	0.25
C	26.6	32.0	0.46	0.34	0.23	0.88	0.81	0.59	0.49	0.33	0.34	0.48	0.35	0.31
D	25.7	32.6	0.55	0.45	0.35	0.85	0.81	0.60	0.56	0.45	0.51	0.59	0.44	0.45
E	25.5	31.3	0.71	0.56	0.68	0.86	0.82	0.47	0.73	0.60	0.99	0.75	0.55	0.97
F	25.2	28.5	0.98	0.70	0.96	0.85	0.83	0.39	1.01	0.74	1.39	0.98	0.72	1.49

microstructure analysis are summarized in Tables 2 and 3. Parameters $\bar{d}$, d_x and d_y are represented as the diameter of the area-analogue circle – DCIRCLE and intercept lengths in x and y direction – FERETX, Y, respectively. Porosity ε was determined as geometrical porosity (from tablet dimensions) and as microstructural porosity (from microstructure analysis).

According to the results of quantitative microstructural analysis, the porosity of the sintered samples decreased with the sintering temperature, as expected. The higher sintering temperature also resulted in pronounced grain growth. An average particle size of both phases NiO and YSZ is very similar in a green state and at low sintering temperatures. However, an average particle size of NiO exceeds YSZ average particle size at higher sintering temperatures. From this fact, we may deduce that NiO in NiO–YSZ composite sinters first and more intensely. Additionally, with higher sintering temperatures, the grains of both phases became rounder. Relatively small average particle diameters (i.e. 0.1 μm at 1150 °C) would usually mean that exact EDS analysis is impossible, due to insufficient resolution of the instrument. However, with careful sample preparation, precise microscopy and, above all, the use of the CAMEO function in INCA software which enables coloring of grains according to their chemical composition, distinguishing between NiO and YSZ became feasible (Fig. 5). From such colorized pictures different gray values for NiO and YSZ can be easily obtained.

The two most apparent differences between sintered and reduced samples are in the increased porosity, and in the increased Ni relative to NiO particle size. One well-known fact when describing the microstructure of the Ni–YSZ anode cermet layer is that its appropriate porosity is between 30 and 40% [32–35]. Considering that about 41.1% of initial volume of NiO is transformed into pores during NiO reduction to Ni, the porosity of the sintered bodies should be close to 10%. Bearing in mind that for high TPB value an average particle size of both phases should also remain as small as possible and that for suitable electrical properties contact between particles should be good, the sintering temperature for sample B was chosen as the most appropriate preparation procedure. A sintering temperature of 1150 °C (sample A) may be considered too low due to the clear microstructure instability of the final Ni–YSZ cermet which was characterized as exaggerated Ni-coarsening. Sintering temperatures higher than 1200 °C, in contrast, will enlarge the average grain size of each phase without substantial improvement of the microstructure stability, which is an undesirable process when preparing nano-scaled Ni–YSZ composite. The final average particle sizes of Ni and YSZ in sample B, 0.27 μm and 0.17 μm respectively, are relatively large compared to the initial NiO–YSZ mixture after the synthesis. However, the nano-sized initial oxide mixture and careful powder treatment enabled the preparation of well sintered bodies with relative densities above 90% in addition to subsequently reduced cermets in which the average particle sizes of both phases are still well within the sub-micrometer range.

A more in-depth image analysis was performed using the line intercept method. Using this method, we obtained information about the number of contact points N_L between

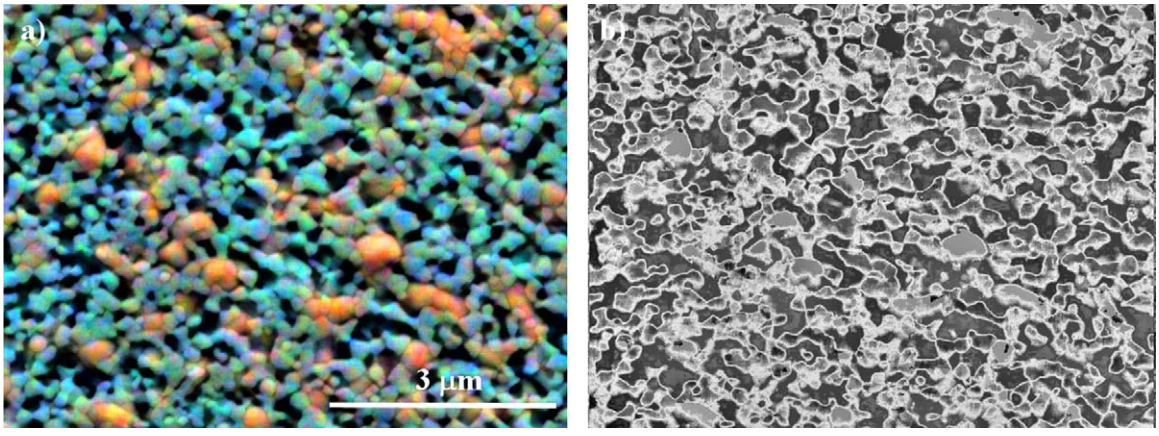

Fig. 5. The obtained SEM micrographs of sample B after the reduction using INCA software (a) and optimized digital grayscale same image (b).

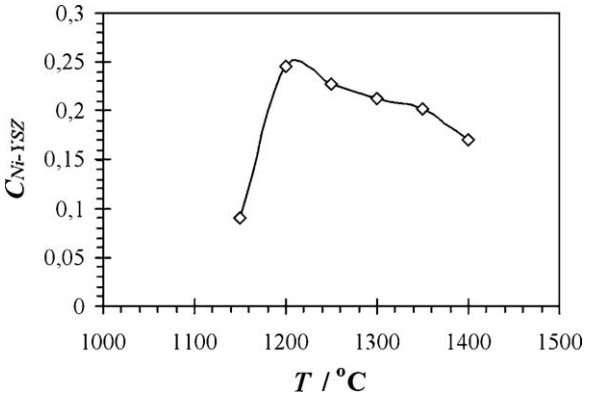

Fig. 6. Contiguity of Ni–YSZ in cermets submitted to various sintering temperatures.

grains of one phase or between grains of different phases in a unit length. However, since all these parameters gave only two-dimensional information, 2D to 3D data transformation was done according to the Gurland principle [36,37] and modified as suggested by Lee et al. [38] based on quantitative microscopic theory [36,37,39], Lee modified Gurland's equation so that a three-phase composite (Ni, YSZ and pores) can be described as follows:

$$C_{\alpha\alpha} = \frac{2N_{L_{\alpha\alpha}}}{2N_{L_{\alpha\alpha}} + N_{L_{\alpha\beta}} + N_{L_{\alpha\gamma}}} \quad (1)$$

$$C_{\alpha\beta} = \frac{N_{L_{\alpha\beta}}}{2N_{L_{\alpha\alpha}} + N_{L_{\alpha\beta}} + N_{L_{\alpha\gamma}} + 2N_{L_{\beta\beta}} + N_{L_{\beta\gamma}}} \quad (2)$$

In the above equations, symbols α, β and γ represent three phases Ni, YSZ and pores, respectively, $N_{L_{\alpha\alpha}}$, $N_{L_{\alpha\beta}}$, $N_{L_{\alpha\gamma}}$, $N_{L_{\beta\beta}}$ and $N_{L_{\beta\gamma}}$ are the number of contact points in a unit length between adequate phases, and $C_{\alpha\alpha}$ and $C_{\alpha\beta}$ are the contiguities which represent a degree of contact of adequate phases in a three-phase mixture. A similar approach to three-dimensional structural information was also proposed by Simwonis et al. [40] calculation of the contiguity between Ni and YSZ revealed interesting and somehow expected results: the highest $C_{\mathrm{Ni-YSZ}}$ value was obtained in the case of sample B which was sintered at 1200 °C (Fig. 6). This phenomenon was ascribed to the relatively small one-phase dominance in the final Ni–YSZ cermet. An average Ni grain in the final sample B was calculated to be much smaller than an average Ni grain in the sample A. At the same time, the average YSZ grain did not grow too extensively when comparing samples A and B. Additionally, poor chemical affinity between Ni and YSZ and excessive Ni sintering due to relatively loose ceramic framework in sample A reduced the number of contact points in a unit length between Ni and YSZ ($N_{L_{\mathrm{Ni-YSZ}}}$ value). With a relatively low $N_{L_{\mathrm{Ni-YSZ}}}$ value, $C_{\mathrm{Ni-YSZ}}$ also decreased. $C_{\mathrm{Ni-YSZ}}$ values calculated for samples C–F relative to the $C_{\mathrm{Ni-YSZ}}$ value for sample B are again lower. This may be understood with respect to the microstructure development during the sintering process. Since NiO and YSZ sinter separately, growth of one-phase dominance reduces the N_L value between different phases and increases the N_L value between grains in one-phase region. From this point of view, preparation parameters for sample B were again chosen as the most appropriate synthesis path for obtaining sub-micrometer Ni–YSZ cermets with a relatively highly-expressed TPB area.

4. Conclusions

Nano-sized NiO–YSZ composites were synthesized with citrate–nitrate combustion of the initial reactive mixture. The average crystallite size after the synthesis for the two phases was estimated to be 6.5 ± 2 nm. Such crystallites, partially agglomerated into soft agglomerates, were also the starting material for the investigations of microstructure development during the sintering. Relatively dense bodies ($\rho_{rel.}$ 91.4%) were prepared at sintering temperatures as low as 1200 °C. Higher sintering temperatures did not significantly increase relative sintered density. A sintering temperature of 1150 °C was recognized as insufficient due to clear microstructure instability during further thermal treatment of the composite. The average grain size of YSZ phase was influenced by the sintering process and was enlarged with the increasing sintering temperature. NiO grains also grew with increasing sintering temperature; however, the dimensions of the final Ni grains formed during the reduction were very much influenced by the microstructure stability of the YSZ framework established during sintering. The smallest Ni grains, still well in a sub-micrometer range ($\bar{d}$ 0.27 μm), as well as the highest contiguity value between Ni and YSZ phases were obtained in the sample sintered at 1200 °C. Smaller $C_{\mathrm{Ni-YSZ}}$ values calculated for samples sintered at 1150 °C or temperatures higher than 1200 °C were ascribed to relatively larger Ni grains or the increased one-phase dominance region of both phases.

References

[1] N.Q. Minh, Ceramic fuel cells, J. Am. Ceram. Soc. 76 (1993) 563–588.
[2] H. Tu, U. Stimming, Advances, aging mechanism, and lifetime in solid oxide fuel cells, J. Power Sources 127 (2004) 284–294.
[3] S. Primdahl, M. Mogensen, Durability and thermal cycling of Ni/YSZ cermet anodes for SOFC, J. Appl. Electrochem. 30 (2000) 247–257.
[4] D. Waldbilling, A. Wood, D.G. Ivery, Electrochemical and microstructural characterization of the redox tolerance of solid oxide fuel cell anodes, J. Power Sources 145 (2) (2005) 206–215.
[5] D. Simwonis, F. Tietz, D. Stover, Nickel coarsening in annealed Ni/8YSZ anode substrates for solid oxide fuel cells, Solid State Ionics 132 (3–4) (2000) 241–251.
[6] J.H. Kim, R.H. Song, K.S. Song, S.H. Hyun, D.R. Shin, H. Yokokawa, Fabrication and characteristics of anode-supported flat-tube solid oxide fuel cell, J. Power Sources 122 (2) (2003) 138–143.
[7] I.C. Vinke, R. Erben, R.H. Song, J. Kiviaho, Installation and operation of kW-class stacks from Jülich in external laboratories, in: Proceedings of the Seventh European SOFC Forum, Lucerne, Switzerland, (2006), p. B036.
[8] N. Nakagawa, K. Nakajima, M. Sato, K. Kato, Contribution of the internal active three-phase zone of Ni-zirconia cermet anodes on the electrode performance of SOFCs, J. Electrochem. Soc. 146 (4) (1999) 1290–1295.
[9] S. Primdahl, B.F. Sørensen, M. Mogensen, Effect of nickel oxide/yttria stabilized zirconia anode precursor sintering temperature on the properties of solid oxide fuel cells, J. Am. Ceram. Soc. 83 (3) (2000) 489–494.
[10] J.H. Yu, G.W. Park, S. Lee, S.K. Woo, Microstructural effect on the electrical and mechanical properties of Ni-YSZ cermet for SOFC anode, J. Power Sources 163 (2007) 926–932.

[11] S.D. Kim, H. Moon, S.H. Hyun, J. Moon, J. Kim, H.W. Lee, Nano-composite materials for high-performance and durability of solid oxide fuel cells, J. Power Sources 163 (2006) 392–397.
[12] M. Mogensen, S. Skaarup, Kinetic and geometric aspects of solid oxide fuel cell electrodes, Solid State Ionics 86–88 (1996) 1151–1160.
[13] P. Costamagna, P. Costa, V. Antonucci, Micro-modelling of solid oxide fuel cell electrodes, Electrochem. Acta 43 (3–4) (1998) 375–394.
[14] F.P.F. van Berkel, F.H. van Heuveln, J.P.P. Huijsmans, Characterization of solid oxide fuel cell electrodes by impedance spectroscopy and *I–V* characteristics, Solid State Ionics 72 (2) (1994) 240–247.
[15] Q. Xue, The influence of particle shape and size on electric conductivity of metal–polymer composites, Eur. Polym. J. 40 (2) (2004) 323–327.
[16] F.H. Wang, R.S. Guo, Q.T. Wei, Y. Zhou, H.L. Li, S.L. Li, Preparation and properties of Ni/YSZ anode by coating precipitation method, Mater. Lett. 58 (24) (2004) 3079–3083.
[17] K. Sato, H. Abe, T. Misono, K. Murata, T. Fukui, M. Naito, Enhanced electrochemical activity and long-term stability of Ni-YSZ anode derived from NiO-YSZ interdispersed composite particles, J. Eur. Ceram. Soc. 29 (2009) 1119–1124.
[18] T. Kawada, N. Sakai, H. Yokokawa, M. Dokiya, M. Mori, T. Iwata, Structure and polarization characteristics of solid oxide fuel cell anodes, Solid State Ionics 40 (41) (1990) 402–408.
[19] J. Mizusaki, H. Tagawa, T. Saito, K. Kamitani, T. Hirano, S. Ehara, T. Takagi, T. Hikita, M. Ipponmatsu, S. Nakagawa, K. Hoshimoto, Preparation of nickel pattern electrodes on YSZ and their electrochemical properties in H_2-H_2O atmospheres, J. Electrochem. Soc. 141 (8) (1994) 2129–2134.
[20] M. Marinšek, K. Zupan, J. Maček, Jadran, Preparation of Ni-YSZ composite materials for solid oxide fuel cells anodes by gel-precipitation method, J. Power Sources 86 (1–2) (2000) 383–389.
[21] F.H. Wang, R.S. Guo, Q.T. Wei, Y. Zhou, H.L. Li, S.L. Li, Preparation and properties of Ni/YSZ anode by coating precipitation method, Mater. Lett. 58 (2004) 3079–3083.
[22] T. Fukui, S. Ohara, M. Naito, K. Nogi, Synthesis of NiO-YSZ composite particles for an electrode of solid oxide fuel cells by spray pyrolysis, Powder Technol. 132 (2003) 52–56.
[23] Y.S. Yoon, J.M. Im, D.W. Shin, Microstructure and electrical conductivity of NiO-YSZ nano-powder synthesized by aerosol flame deposition, Ceram. Int. 34 (4) (2008) 873–876.
[24] A. Ringuede, J.A. Labrincha, J.R. Frade, A combustion synthesis method to obtain alternative cermet materials for SOFC anodes, Solid State Ionics 141–142 (2001) 549–557.
[25] P. Duran, J. Tartaj, F. Capel, C. Moure, Processing and characterization of a fine nickel oxide/zirconia/composite prepared by polymeric complex solution synthesis, J. Eur. Ceram. Soc. 23 (2003) 2125–2133.
[26] A. Ringuede, J.R. Frade, J.A. Labrincha, Combustion synthesis of zirconia-based cermet powders, Ionics 6 (2000) 273–278.
[27] S.T. Aruna, M. Muthuraman, K.C. Patil, Synthesis and properties of Ni-YSZ cermet: anode material for solid oxide fuel cells, Solid State Ionics 111 (1998) 45–51.
[28] S.J. Kim, C.H. Jung, Y.S. Kim, Synthesis of Ultrafine NiO-YSZ Powders by GNP (Glicine Nitrate Process), B. Thorstensen (Ed.), in: Proceedings of the 2nd European Solid Oxide Fuel Cell Forum, Oslo, Druckerei J. Kinzel, Gottingen, 1 (1996) 321-330.
[29] P. Courty, H. Ajot, C. Marcilly, B. Delmon, Highly dispersed mixed oxides on oxide solid solutions obtained by pyrolysis of amorphous precursors, Powder Technol. 7 (1) (1973) 21–38.
[30] M. Marinšek, K. Zupan, J. Maček, Citrate-nitrate gel transformation behaviour during the synthesis of combustion derived NiO-YSZ composite, J. Mater. Res. 18 (7) (2003) 1551–1560.
[31] C. Clausen, C. Bagger, J.B. Bilde-Sorensen, A. Horsewell, Microstructural and microchemical characterization of the interface between $La_{0.85}Sr_{0.15}MnO_3$ and Y_2O_3-stablized ZrO_2, Solid State Ionics 70–71 (1994) 59–64.
[32] W. Hu, H. Guan, X. Sun, S. Li, M. Fukumoto, I. Okane, Electrical and thermal conductivities of nickel-zirconia cermets, J. Am. Ceram. Soc. 81 (8) (1998) 2209–2212.
[33] D.W. Dees, T.D. Claar, T.E. Easčer, D.C. Fee, F.C. Mrazek, Conductivity of porous Ni/ZrO_2-Y_2O_3 cermets, J. Electrochem. Soc. 134 (9) (1987) 2141–2146.
[34] T. Kawashima, M. Hishinuma, Analysis of electrical conduction paths in Ni/YSZ participate composites using percolation theory, Mater. Trans. 37 (7) (1996) 1397–1403.
[35] U. Anselmi-Tamburini, G. Chiodelli, M. Arimondi, F. Maglia, G. Spinolo, Z.A. Munir, Electrical properties of Ni/YSZ cermets obtained by combustion synthesis, Solid State Ionics 110 (1998) 35–43.
[36] J. Gurland, The measurement of grain contiguity in two phase alloys, Trans. Metall. Soc. AIME 212 (1958) 452–455.
[37] J. Gurland, An estimate of contact and contiguity of dispersions in opaque samples, Trans. Melall. Soc. AIME 236 (1966) 642–646.
[38] J.H. Lee, H. Moon, H.W. Lee, J. Kim, J.D. Kim, K.H. Yoon, Quantitative analysis of microstructure and its related electrical property of SOFC anode, Ni-YSZ cermet, Solid State Ionics 148 (2002) 15–26.
[39] Z. Fan, A microstructural approach to the effective transport properties of multiphase composites, Phil. Mag. A 73 (1996) 1663–1684.
[40] D. Simwonis, F. Tietz, D. Stoever, Nickel coarsening in annealed Ni/8YSZ anode substrates for solid oxide fuel cells, Solid State Ionics 166 (2000) 241–251.